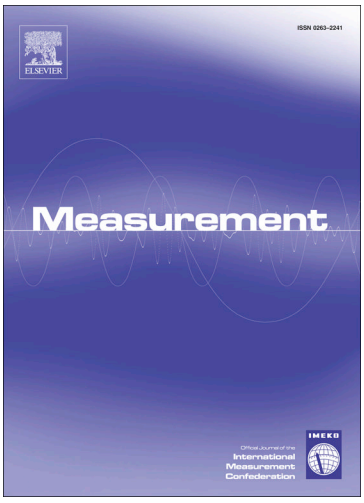

Dielectric Spectroscopy Measurements on Kaolin Suspensions for Sediment Concentration Monitoring

Partha Narayan Mishra, Thierry Bore, Yucheng Jiang, Alexander Scheuermann, Ling Li

PII: S0263-2241(18)30133-7
DOI: https://doi.org/10.1016/j.measurement.2018.02.034
Reference: MEASUR 5282

To appear in: *Measurement*

Received Date: 16 January 2018
Revised Date: 10 February 2018
Accepted Date: 19 February 2018

Please cite this article as: P. Narayan Mishra, T. Bore, Y. Jiang, A. Scheuermann, L. Li, Dielectric Spectroscopy Measurements on Kaolin Suspensions for Sediment Concentration Monitoring, *Measurement* (2018), doi: https://doi.org/10.1016/j.measurement.2018.02.034

Dielectric Spectroscopy Measurements on Kaolin Suspensions for Sediment Concentration Monitoring

Partha Narayan Mishra[1]; Thierry Bore[2]; Yucheng Jiang[3], Alexander Scheuermann[4] and Ling Li[5]

[1]Doctoral Research Scholar
Geotechnical Engineering Center
School of Civil Engineering
The University of Queensland
St Lucia-4072, QLD, Australia

[2]Postdoctoral Research Fellow
School of Civil Engineering
The University of Queensland
St Lucia-4072, QLD, Australia

[3]Former Undergraduate Student
School of Civil Engineering
The University of Queensland
St Lucia-4072, QLD, Australia

[4]Associate Professor and Deputy Centre Director
Geotechnical Engineering Center
School of Civil Engineering
The University of Queensland
St Lucia-4072, QLD, Australia

[5]Professor of Environmental Engineering
School of Civil Engineering
The University of Queensland
St Lucia-4072, QLD, Australia

Corresponding author: Partha Narayan Mishra; Email: p.mishra@uq.edu.au

Abstract:

Sedimentation along with consolidation processes dictate the in situ engineering and hydraulic behavior of a particulate system such as soil. With this in view, the present investigation discusses about the application of dielectric measurements in relation to sediment concentration measurements for fine grained soils. An in-house set up comprising of open ended coaxial probes and vector network analyzer has been used to measure the dielectric behavior of kaolin suspensions in tap and deionized water. These have been further analyzed to furnish suspended sediment concentration, pore water conductivity and shape factors utilizing *Complex Refractive Index Model* (CRIM) and *Bruggeman–Hanai–Sen* (BHS) model, through the implementation of an optimization scheme. Furthermore, measured and estimated suspended sediment concentrations showed good agreement with each other in terms of statistical parameters, and a ranking of models approach reliant on three statistical criteria revealed that, CRIM outperforms BHS model for estimating sediment concentrations.

Keywords: Measurement; Concentration; Kaolin; Dielectric; Coaxial probes; Statistical Analysis

1. INTRODUCTION

Weathering of rocks, and subsequent deposition of uncemented aggregates at their sites of origin (residual deposition), or in places far from their origin (transported deposition via air, water, gravity etc.) lead to formation of geomaterials. In general, the tendency of particles to settle down in a suspension, which is either controlled by particular self-weight as in case of coarse grained soils, or by a critical combination of inter-particle attractive and repulsive forces as in case of fine grained soils [1], is commonly known as sedimentation [2]. Sedimentation behavior of clay mineral rich materials such as kaolinite, bentonite etc. are particularly of interest to fraternities in colloidal chemistry and soil science, as these materials are primarily made up of fine reactive particulates.

The reactive nature of clay minerals may be ascribed to unsatisfied ion valences, and presence of net negative charges on the surface. As such, during the process of sedimentation, clays might attain either dispersed or flocculated state depending on the dominant interparticular force. Fine grained clay mineral such as kaolinite, illite, montmorillonite [3,4] rich depositions existing undisturbed for a long period of time tend to adopt either an 'edge to face' (in non-saline pore fluid) or 'face to face' (in saline pore fluid) flocculated configuration which attributes to their high strength and permeability with low collapsibility [5,6]. Therefore, sedimentation along with consolidation processes dictate the in situ engineering and hydraulic behavior of a particulate system such as soil. As such, application of sedimentation in geoengineering prospective pertains to delineation of 'soil' as understood in conventional geotechnical engineering in a dispersion system [7], mechanism of strength development in soil deposits [8], landfill technology [9], metal recovery from laterite slurries [10], mine tailing dams [11], management of fine fractions [12] and dredged material form ports and harbors, borehole stability, etc.

In an aqueous media, settling velocity is one of the characteristic properties of the sediment, which is reliant on the properties of the media such as density & viscosity, along with particular properties such as size, shape, density and concentration/ number [13]. Furthermore, sediment concentration measurement and monitoring is also used as a tool for predicting erosion in moderate slopes [14], for estimation of contaminant, nutrient and metals carried by sediment loads in rivers [15,16] and forms an significant aspect pertaining to channel navigability, longevity of hydroelectric equipment, fish habitat [17]. Moreover, applications also extend to several major applied sciences and engineering fields such as

metallurgical engineering [18] ,biological sciences [19], ceramic engineering [20], chemical processing [21], hydrogeological engineering [22] etc.

Although, measurement of suspended particular/sediment concentration can be carried out either by direct sampling [23,24] or through indirect surrogate methods [25-27], the later ones are usually preferred owing to the spatial and temporal variability, labour, expense and several other difficulties associated with the former one [26,28]. Acoustic methods rely on the strength of the back scattered signal from sediments incident with high frequency sound waves from transducers, to estimate particle size and concentration. While the method provides appreciable spatial and temporal resolution, converting the back scattered signal to sediment properties is rather difficult [25]. Laser signals can be used either by the focused beam reflectance [29] or laser diffraction [30] technique. Both the methods are independent of particle sizes. However, they are quite expensive to be implemented, and are intrusive to the flow. For sampling over broad areas, the amount of reflected radiation measured by a spectrometer can be linked to concentration of suspended sediments [31]. However, spectral reflectance method suffers from limited resolution of measurement and particle size dependency. Recently, Chung and Lin [32], Lin et al. [28] proposed an improvised technique for suspended sediment concentration (SSC) measurement through time domain reflectometry (TDR) method, which can also be used to measure porosity in granular materials [33], soil moisture measurement [34] etc. The method is based on classic flight time interpretation of a TDR waveform in combination with biphasic (water-sediment suspension) volumetric mixing equation (Complex Refractive Index Model, CRIM) [35,36]. This method is economic and provides an improvised range and resolution.

However, TDR measurements present several limitations. The analysis is based on the determination of effective parameter, computed from the TDR waveform, such as effective permittivity ε_{app} . It is well known that the dieletric permittivity of soil is a complex quantity and is frequency depandent [37]. In this context, the amount of informations accessible by TDR method is considerably reduced. Furthermore, this apparent permittivity is dependant on many factors such ase probe design, cable resistivity, cable length etc. [38,39]. Also, a specific calibration has to be performed for each type of sensor which in turn multiply the number of measurements.

In view of the above, we propose a dielectric spectroscopy based approach in frequency domain to measure suspended sediment concentration for fine-grained porous media. The primary driveway for the investigation is to combine frequency domain measurements in microwave range [40] with bi-phasic mixing equations [41] in an optimization scheme to

achieve simultaneous and multi parameter estimations. Different mixing models are tested and systematically compared (CRIM, Bruggeman Hanai Sen model) in order to achieve SSC and pore water conductivity [42,43] estimations.

2. MATERIALS AND METHODOLOGY

2.1 Materials

For the present investigation, a commercial grade kaolin (Eckalite-I) procured from an Australia based business was used.

2.1.1 Physico-geotechnical characterization:

Particular composition of the kaolin was determined by wet analysis through laser diffraction measurement using a particle size analyzer (Malvern Mastersizer2000 MU). In a suspension, the mastersizer determines volume of different sized particles present from measurement of light scattering of particles. This method provides a rather continuous, fast and accurate measurement, and is advantageous over conventionally used hydrometer analysis for establishing particle size distribution curve (PSD) of kaolin [44]. PSD of kaolin, as an average of 5 sets of measurements, is reported in Fig.1. As shown in Fig. 1, the sigmoid shaped PSD reveals, uniformity coefficient ($C_u=D_{60}/D_{10}$) and coefficient of curvature ($C_c= D_{30}^2/ D_{60}\times D_{10}$) of the kaolin sample are 5.1 and 1.1, respectively. Therefore, it is well graded. Furthermore, clay sized fraction (<2µm) and silt sized fraction (>2µm, <63µm) in the sample were observed to be 6% and 91%, respectively. Occurrence of large proportion of silt sized fraction may be attributed to flocculation [45]. Moreover, consistency limits and specific gravity of kaolin were determined as per the relevant codal provisions and are summarized in Table 1 [46].

2.1.2 Chemo-mineralogical characterization:

Upon subjection to X-ray diffraction and total elemental microwave digestion, it was identified that the kaolin sample has 72.7% of reactive clay minerals (52.7% kaolinite and 20% Illite-mica) [46]. Total Specific surface area (total surface area per unit dry mass of soils) of the sample determined with BET and single point differential method is 16.86 m^2/g [46]. Furthermore, cation exchange capacity (amount of exchangeable cations that soil can accommodate) of the sample determined by means of silver thiourea methods is 26.5 meq/100g [46]. These parameters indicate that, the sample is rich in reactive minerals, and is

expected to undergo changes in geotechnical parameters when subjected to alteration in concentration of pore fluid.

2.2 Methodology

2.2.1 Measurement of dielectric properties of the material:

An in-house setup involving open ended coaxial probes and a vector network analyser [47] has been used to establish the frequency dependent dielectric response [48] of the material. The vector network analyser (VNA) as represented in Fig. 2, sends through incident signals from the port(s) followed by receiving and processing back the reflected and (or) transmitted signals from the material under investigation; the 'to' and 'fro' signals are correlated with scattering parameters [46].

In order to minimise the systematic errors, *Open*, *Short*, *Load* calibrations were performed during a one port measurement based on open ended coaxial probes [49]. The in house probe was made out of a 'N' type connector with diameter of outer and inner conductor as 5mm and 3mm, respectively, which is housed inside a sample holder of 70 mm diameter (Fig.3). Based on a bilinear relationship, scattering function (S_{11}) is correlated to the relative complex permittivity ($\varepsilon^*_{r,eff}$) as per Eq. 1 [50]:

$$\varepsilon^*_{r,eff} = \frac{C_1(\omega)\bullet S_{11}(\omega) - C_2(\omega)}{C_3(\omega) - S_{11}(\omega)} \tag{1}$$

where, ω is the angular frequency and c_i are the complex calibration constants evaluated from Open-Water-Liquid (OWL) calibration suggested by Wagner et al. [51]. Designating *O*, *W* and *L* in superscripts for the parameters associated with Open (air), Water and Liquid, respectively, following system of Eq. can be written based on Eq. 1.

$$\left.\begin{array}{llll} S^O_{11}(\omega)\bullet C_1(\omega) & -C_2(\omega) & -\varepsilon^{*O}_{r,eff}(\omega)\bullet C_3(\omega) = -\varepsilon^{*O}_{r,eff}(\omega)\bullet S^O_{11}(\omega) \\ S^W_{11}(\omega)\bullet C_1(\omega) & -C_2(\omega) & -\varepsilon^{*W}_{r,eff}(\omega)\bullet C_3(\omega) = -\varepsilon^{*W}_{r,eff}(\omega)\bullet S^W_{11}(\omega) \\ S^L_{11}(\omega)\bullet C_1(\omega) & -C_2(\omega) & -\varepsilon^{*L}_{r,eff}(\omega)\bullet C_3(\omega) = -\varepsilon^{*L}_{r,eff}(\omega)\bullet S^L_{11}(\omega) \end{array}\right\rangle \tag{2}$$

In a matrix form, Eq. 2 can be rewritten as:

$$\begin{bmatrix} S^O_{11}(\omega) & -1 & -\varepsilon^{*O}_{r,eff}(\omega) \\ S^W_{11}(\omega) & -1 & -\varepsilon^{*W}_{r,eff}(\omega) \\ S^L_{11}(\omega) & -1 & -\varepsilon^{*L}_{r,eff}(\omega) \end{bmatrix} \begin{bmatrix} c_1(\omega) \\ c_2(\omega) \\ c_3(\omega) \end{bmatrix} = \begin{bmatrix} -\varepsilon^{*O}_{r,eff}(\omega)\bullet S^O_{11}(\omega) \\ -\varepsilon^{*W}_{r,eff}(\omega)\bullet S^W_{11}(\omega) \\ -\varepsilon^{*L}_{r,eff}(\omega)\bullet S^L_{11}(\omega) \end{bmatrix} \tag{3}$$

Frequency dependent measurements for air, deionised water and methanol were used to determine c_i in Eq, 3. For air, a value of permittivity equal to 1 over the whole frequency was used. Deionised water has been extensively studied in literature over last decades. It has been shown that the frequency dependent dielectric permittivity [52] can be modelled with a Debye function (Eq.4).

$$\varepsilon_W(\omega,T) = \varepsilon_\infty(T) + \frac{\Delta\varepsilon_W(T)}{1+ j\omega\tau_W(T)} \quad (4)$$

where, ε_∞ denotes the high frequency limit of real part of the relative permittivity, relaxation strength $\Delta\varepsilon_w = \varepsilon_s - \varepsilon_\infty$ with quasi static real relative permittivity ε_s and the relaxation time τ_w. The temperature dependent relaxation strength $\Delta\varepsilon_w$ and ε_∞ are computed according to Ellison [53], whereas temperature dependent dielectric relaxation time τ_w is calculated according to Kaatze [54].Finally, the frequency dependent permittivity of methanol as a function of temperature was computed from the extensive data base presented in Gregory and Clarke [55].

Performance of the calibrations were further appraised with other standard liquids (tap water, ethanol etc.), and a satisfactory estimation of relative complex permittivity was obtained for 50 MHz - 3GHz range.

2.2.2 Sample Preparation:

Prior to the test, kaolin samples were kept inside an oven at 60°C for 24 hr to eliminate any initial residual moisture. Masses of the kaolin sample needed to achieve several target concentrations in deionised water and tap water, as detailed in Table 2, based on a sample container of 60 ml volume was calculated. After adding the required mass of kaolin, the containers were filled with the respective solvent, shaken well and stored for a period of 24 hr. Just before testing the samples, the containers were shaken well again and poured into the the sample holders fitted with previously calibrated dielectric probes (Fig. 3), to record the frequency dependent dielectric response. With a handheld multi parameter measuring device (Oakton™ PCSTestr 35), electrical conductivity (σ_{sp}), total dissolved solid (TDS) and salinity of the suspensions were measured. Fig. 4 (a), (b) and (c) reveal that, with increase in kaolin concentration in the suspension, $\sigma_{sp,}$ TDS and salinity increase. After the dielectric and characterization measurements, samples were put back inside the oven, and concentrations of all the suspensions were measured through gravimetric method. Fig. 5 (a) and (b) present a plot between target and measured concentration of kaolin in deionized and tap water. It is

observed that, both are close to each other with majority of data points lying on and vicinity of 1:1 line. This validates the target concentrations match with the achieved measured concentration confirming the eligibility of the chosen procedure.

2.2.3 Broadband electromagnetic modeling approach:

It is worth mentioning that electromagnetic methods in general provide a means to perform indirect soil characterization by correlating the electric permittivity and the targeted soil parameters. To do so, different approaches are available: empirical calibration, relaxation model and theoretical mixing rules. Empirical calibrations are widely used in Time Domain Reflectometry application, with the classic and well known examples of the determination of water content from apparent permittivity with Topp et al. [56]'s approach. As explained before, the major drawback of the method is that, this calibration is specific to a material and a sensor. Moreover, the correction of temperature on apparent permittivity computed from TDR waveform with empirical calibration remains challenging [57,58]. Relaxation models have been widely used for soils [59,60] or suspensions [61] to model the spectrum as a sum of relaxation processes along the frequency bandwidth. The parameters for each process are computed by matching the spectrum and the model. Although this method presents statistically good results in terms of fitting, the attribution to each relaxation process to physical phenomena is still debateable [62]. Moreover, relaxation model offers a powerful tool to probe the interaction between water and solid phases through relaxation processes, but it remains complicated to directly link relaxation parameters with state parameters such as water content or porosity. Theoretical mixing equations consider the soil as a porous medium consisting of solid particles, pore air and pore water phases. The electric permittivity of each phase can be computed independently, whereas the dielectric properties of the soil is computed according to a mixing rule [63, 64]. The major advantage associated with this method is the ability to take into account the frequency and temperature dependency of individual phases. Moreover, the mixing equations allow the dielectric properties of the soil to be expressed as functions of state parameters such as water content and porosity. Although, simplification of the soil structure as well as the difficulty to integrate interaction between individual phases [65] is a known drawback, in the case of suspensions, only water and solid phase exist which considerably simplifies the formulation.

For the pore water, a modified Debye model [66] was used to take into account the temperature and frequency dependency:

$$\varepsilon_W(\omega,T,\sigma_w)=\varepsilon_\infty(T)+\frac{\Delta\varepsilon_W(T)}{1+j\omega\tau_W(T)}-j\frac{\sigma_W}{\omega\varepsilon_0} \quad (5)$$

where σ_W is the direct current conductivity. Please note that the modified Debye preserves the classic Debye model (Eq.4) with a direct current contribution to take into account conductivity loss. Thus, the same notation and temperature dependant functions are used here.

The dielectric response of solid phase is assumed to be independent of frequency and temperature, and the electric permittivity of solid phase ε_s is derived from solid density ρ_G with Eq.6 [67].

$$\varepsilon_S=(1.01+0.44.\rho_G)^2-0.0062 \quad (6)$$

Finally, the dielectric properties of the suspension can be computed with the following equations

$$\varepsilon_{CRIM}(n,\omega,T,\rho_G,\sigma_W)=\left(n(\varepsilon_W)^{0.5}+(1-n).(\varepsilon_S)^{0.5}\right)^{(1/0.5)} \quad (7)$$

$$\left(\frac{\varepsilon_S-\varepsilon_{BHS}(\omega,T,n,\rho_G,\sigma_W)}{\varepsilon_S-\varepsilon_W}\right).\left(\frac{\varepsilon_W}{\varepsilon_{BHS}(\omega,T,n,\rho_G,\sigma_W)}\right)^{\alpha}=n \quad (8)$$

where, *n* the porosity which can be linked to the concentration with the following relation:

$$(1-n)\rho_G=c \quad (9)$$

2.2.4 Optimisation scheme:

In this framework, the unknown parameters of the models were derived by fitting the computed spectra in an optimization scheme. A Monte Carlo Markov Chain (MCMC) algorithm was used to obtain the best fit [35,68]. In this algorithm, for the unknown parameters, a series of MCMC samples following a Gaussian-likelihood-based posterior distribution are generated by using a Gibbs sampling method [69]. Then, posterior-mean parameter estimations, obtained by averaging over these samples, are used to get the best fit between the measurements and outputs of the modelling through Eq. 7 and 8. The needed information is a lower and upper bound and a starting guess for each of the parameters.

In the case of CRIM, 2 parameters were computed: the concentration *c* and the pore water conductivity σ_W; whereas in the case of BHS model 3 parameters were determined: the

concentration c and the pore water conductivity σ_W and the exponent α. Please note that the temperature was measured during the test and used here as input (temperatures were ranging 23°C to 25.3°C).

2.2.5 Ranking of Models:

In order to evaluate the relative efficacy of the CRIM and BHS model in prediction of concentration of suspensions, a ranking system reliant on several statistical parameters through three criteria [70] has been used. In this method, each model is assigned a numeric rank (1 or 2) adjudged for each set of statistical criterion. Ranking Index (RI) of the model is worked out as the sum of its ranks resulting out of individual statistical criterion. The model with the smallest RI is the best model or holistically ranked high in terms of prediction efficiency.

The three sets of statistical criteria used are described in brief below:

- Criterion 1: (R1), Based on coefficient of determination (R) and Nash-Sutcliff coefficient of efficiency (E)

  Coefficient of determination (R) has been shown to be a biased estimate of efficacy of a model [71]. Therefore, Nash-Sutcliff coefficient of efficiency (E) based on Eq. 10 is also used in performance assessment of the model.

$$E = 1 - \frac{\sum (C_i - C_{i,est})^2}{\sum (C_i - C_{mean})^2} \tag{10}$$

  where, C_i, $C_{i,est}$ and C_{mean} are the observed concentrations, estimated concentrations and mean concentration of suspensions respectively. Models are ranked based on closeness of R and E values to 1. Models with closest R and E values to 1 are ranked higher than the others.

- Criterion 2: (R2), Based on mean (μ) and standard deviations (SD) of the ratio of estimated to observed concentrations

  An estimation model, under idealised conditions, produces estimates such that the mean (μ) and standard deviations (SD) of ratio of estimated to measured values are 1.0 and 0, respectively. μ values >1 and <1 signify over and under prediction, respectively [72]. Based on the above concept, the model having μ and SD value close to 1.0 and 0, respectively, is ranked higher than the other one.

- Criterion 3: (R3), Based on the cumulative probability of the ratio of estimated to observed concentrations

  Under this criterion, ratio of estimated to observed concentrations are sort in ascending order and plotted against the cumulative probability (*P*) calculated as per Eq. 11.

$$P = \frac{i}{m+1} \tag{11}$$

  where, *i* and *m* are order numbers assigned to ascendingly sort ratios of estimated to observed concentrations, and number of observations, respectively. Ratios of estimated to observed concentrations corresponding to 50% and 90% cumulative probability are referred as P_{50} and P_{90}, respectively. P_{50} is a signifier of under/over prediction for a model and P_{90} implies alteration of ratios of estimated to observed concentrations over the total observations. The model having P_{50} and P_{90} closest to 1 is ranked higher than the others.

Eventually, Ranking Index (RI) is expressed as the sum of the ranks arising out of individual criterion (Eq.12), and the model with least RI is considered to be the best model.

$$RI = R1 + R2 + R3 \tag{12}$$

3. RESULTS AND DISCUSSION

Fig. 6(a) represents the comparison between the measured relative effective complex permittivity $\varepsilon^*_{r,eff(\omega)}$ for kaolin mixed with tap water and the best fit obtained with MCMC algorithm for CRIM and BHS model. Fig. 6(b) represents the corresponding quantity for kaolin mixed with deionized water. To ensure clarity for both pictures, only a selection of the data for 5 samples in each case is shown.

The spectrum presents typical pattern for suspensions. The real part is almost independent of frequency. Nevertheless, for frequencies between 50 MHz and 1 GHz, a systematic relationship between concentration and real part of permittivity can be observed (the highest value of real part of permittivity is obtained for the lowest concentration and vice versa). Real part of the permittivity at 500 MHz versus concentration is plotted in Fig 7(a) and (b) for kaolin with tap water and DI water, respectively. It is interesting to note that a liner relationship with good statistical correlation (R=0.9991 and 0.9962, respectively) can be observed for both sets of measurements. The imaginary part of the spectra is mostly

dominated at low frequency (between 50 MHz and 200 MHz) by a strong direct conductivity contribution. Higher values of the imaginary part can be observed for kaolin mixed with tap water due to salinity losses. Above 1 GHz, the imaginary part started to increase, which can be related to the 'tail' of the free water relaxation. Similar type of behavior have been observed in different studies; for example, organically modified bentonite suspensions were investigated with dielectric spectroscopy [61] over the 200 MHz – 1.2 GHz frequency bandwidth, and a linear relationship between permittivity at 200 MHz and porosity (or concentration as per Eq. 9) was observed. Other studies on clays suspensions noted a similar kind of behavior [73,74], but mostly focused on relaxation behavior.

The parameters estimated with CRIM and BHS model for both sets of measurements are presented in Figs. 8, 9 and 10. From Fig. 8, it is evident and clearly observed that the measured and estimated concentrations by either of the models are in close agreement with each other in terms of statistical parameters and fall in between 95% of confidence and prediction bands. As can be seen from Fig. 9 (a) and (b) the electrical conductivities increased with increase in concentration of both liquids. Samples in tap water yielded naturally a higher pore water conductivity, which followed an increasing trend with increase in concentration.

It is worth reiterating that for CRIM, α is fixed to be 0.5 (refer to Eq. 7). For the BHS model, the shape factor α (refer to Eq. 8) varied with change in concentration, and this is presented in Fig. 10. The values obtained for α ranges from 0.3 and 0.45 (except for KT1 where shape factor is close to 0.1). BHS model can also take into account the influence in shape and orientation of particles shape through the shape factor: $\alpha=1/3$ corresponds to spherical particles, $0 < \alpha < 1/3$ corresponds to prolate spheroids and $1/3 < \alpha < 1$ corresponds to platy spheroids [75]. A general assumption is to consider spherical particles and thus to fix α equal to 1/3 (Sen et al. 1981). The obtained values in this study are mostly higher than 1/3 (only KT1, KT2, KD1 and KD2 are below 1/3). This would mean that the solids particles are more likely to have a shape of platy spheroids. Nevertheless, a systematic analysis involving microstructural characterisation and analysis alongside would be required to investigate this aspect, which is beyond the scope of this paper.

From Fig. 11 (a), a nearly linear relation between the measured electrical conductivity of the suspension σ_{SP} and estimated electrical conductivity of the water phase σ_w can be observed with increase in concentration. This is due to the fact that, σ_w attributes towards the electrical conductivity of the suspension, $\sigma_{SP.}$

As described in the previous section, a ranking analysis was performed, and is summarized in Table 3 to ascertain the relative performance of CRIM and BHS in estimation of the concentration of the suspension. As it can be observed from table 3, CRIM performs better than BHS model for best fit calculations for estimation of concentration of kaolin in tap water. However, BHS model outperforms CRIM in best fit calculations for the corresponding quantity in DI water. Moreover, CRIM performs statistically better than BHS model in terms of μ (closer to 1) and *SD* (closer to 0) for the ratio of estimated to observed concentration of kaolin in tap and DI water. Fig. 12 presents cumulative probability plots for the ratio of estimated (CRIM and BHS model) to measured concentration of kaolin in tap water and DI water, respectively. From Fig. 12 and Table 3, it can be noted that P_{50} and P_{90} of estimated to measured concentration of kaolin in tap and DI water are closer to 1 for CRIM. Considering all the three statistical criteria, holistically, CRIM is observed to perform better than BHS model for the estimation of suspension concentration.

4. SUMMARY AND CONCLUSIONS

This paper introduced and discussed the application of dielectric measurements for determining the suspended sediment concentration of suspensions.

- With the help of an in-house set up comprising of open ended coaxial probes and vector network analyzer, dielectric behavior of kaolin suspensions were measured, which were then analyzed to furnish suspended sediment concentration, pore water conductivity and shape factors.
- CRIM and BHS model were employed to achieve the above mentioned objective through the implementation of an optimization scheme. A linear relationship was observed between real part of the dielectric permittivity at 500 MHz and the concentration. Moreover, real part of the dielectric permittivity is shown to be almost independent of frequency and to reduce with increase in concentration at any given frequency. At low frequencies, higher concentrations yielded higher loss, and thus higher values of imaginary part of the dielectric permittivity.
- Furthermore, measured and estimated suspended sediment concentrations showed good agreement with each other in terms of statistical parameters. A ranking of the models reliant on three statistical criterion revealed that, CRIM performs better than the BHS model in the studies reported herein.

Acknowledgements:

This work was funded by scholarship supports through 'Australian Government Research Training Program Scholarship' (Formerly 'International Postgraduate Research Scholarship'), UQ Centennial Scholarship (The University of Queensland) and Top up scholarship (School of Civil Engineering, The University of Queensland) awarded to Mr. P.N. Mishra. The support through the Port of Brisbane / UQ research venture is gratefully acknowledged. We also thank the anonymous reviewers for their time and suggestions to improve the manuscript.

REFERENCES

1. A.M. Palomino, J.C. Santamarina, Fabric map for kaolinite: effects of pH and ionic concentration on behavior, Clays and Clay Minerals, 53(3) (2005) 209-222.
2. H. van Olphen, An Introduction to Clay Colloid Chemistry, 1st ed., Interscience Publishers, New York. USA, 1963.
3. M. Salavati-Niasari, E. Zamani, M. Bazarganipour, Epoxidation of cyclohexene with K10-montmorillonite and Schiff-base macrocyclic copper complexes, Appl. Clay Sci., 38 (1–2) (2007), 9-16.
4. M. Salavati-Niasari, Synthesis, characterization and catalytic oxidation of cyclohexene with molecular oxygen over host (montmorillonite-K10)/guest (nickel(II) complexes of 12- and 13-membered diaza dioxa Schiff-base macrocyclic ligand) nanocatalyst (HGN), J. Mol. Catal. A: Chem. 263 (2007) 247–252.
5. T.W. Lambe, R.V. Whitman, Soil Mechanics, John Wiliey & Sons, 1969.
6. B.M. Das, Advanced Soil Mechanics, 3rd ed., Taylor and Francis, NY, USA, 2008.
7. E.C. McRoberts, J.F. Nixon, A theory of soil sedimentation, *Canadian Geotechnical Journal* 13(3) (1976) 294-310.
8. D. Perret, J. Locat, S. Leroueil, Strength development with burial in fine-grained sediments from the Saguenay Fjord, Quebec, Canadian Geotechnical Journal 32(2) (1995) 247-262.
9. A. Sridharan, K. Prakash, (1999) Influence of clay mineralogy and pore-medium chemistry on clay sediment formation, Canadian Geotechnical Journal 36(5) (1999) 961-966.

10. S. Azam, R.J. Chalaturnyk, J.D. Scott, Geotechnical Characterization and Sedimentation Behavior of Laterite Slurries, Geotechnical Testing Journal 28(6) (2004) 523-533.
11. G. Blight, Geotechnical Engineering for Mine Waste Storage Facilities, CRC Press, Taylor & Francis, London, UK, 2010.
12. D. Felix, I. Albayrak, R.M. Boes, Continuous measurement of suspended sediment concentration: Discussion of four techniques, *Measurement*, 89 (2016) 44-47.
13. N.S. Cheng, Effect of concentration on settling velocity of sediment particles, J. Hydraulic Engineering 123(8) (1997) 728-731.
14. V. Bagarello, C. Di Stefano, V. Ferro, P.I.A. Kinnell, V. Pampalone, P. Porto, F. Todisco, Predicting soil loss on moderate slopes using an empirical model for sediment concentration, Journal of Hydrology 400 (1-2) (2011) 267–273.
15. A. Helland, The Importance of Selective Transport and Sedimentation in Trend Monitoring of Metals in Sediments. An Example from the Glomma Estuary, East Norway, Water, Air, and Soil Pollution 126(3) (2001) 339-361.
16. P. Gao, Understanding watershed suspended sediment transport, Progress in Physical Geography 32(3) (2008) 243-263.
17. Ö. Kişi, River suspended sediment concentration modeling using a neural differential evolution approach, Journal of Hydrology 389 (1-2) (2010) 227–235.
18. A.S. Michaels, J.C. Bolger, Settling rates and sediment volumes of flocculated kaolin suspensions, *I & E.C. Fundamentals* 1 (1962) 24-33.
19. K. Asami, T. Hanai, Dielectric monitoring of biological cell sedimentation. Colloid & Polymer Science 270 (1992) 78-84.
20. K. Ma, A.C. Pierre, Sedimentation Behavior of a fine kaolinite in the Presence of Fresh Fe Electrolyte, *Clays and Clay Minerals* 40(5) (1992) 586-592.
21. W.K. Mekhamer, N. Al Andis, M. El Shabanat, Kinetic study on the sedimentation behavior of Na- and Ca-kaolinite suspension in the presence of polyethyleneimine, *Journal of King Saud University – Science* 21(2) (2009) 125-132.
22. K. Debnath, S. Chaudhuri, Effect of suspended sediment concentration on local scour around cylinder for clay–sand mixed sediment beds, *Eng. Geol.* 117 (3–4) (2011) 236-245.
23. B.E. Davis, A guide to the proper selection and use of federally approved sediment

and water-quality samplers, U. S. Geol. Surv. Open File Report (2005) 2005 – 1087.

24. J.R Gray, F.J.M. Simo˜es, Estimating sediment discharge, in: M. Garcia (Eds.), Sedimentation Engineering – Processes, Measurements, Modeling, and Practice, Manual 110, ASCE, 2008, pp. 1067 – 1088.
25. D.G. Wren, B.D. Barkdoll, R.A. Kuhnle, R.W. Derrow, Field techniques for suspended sediment measurement, Journal of Hydraulic Engineering 126(2) (2000) 97–104.
26. J.R. Gray, J.W. Gartner, Technological advances in suspended-sediment surrogate monitoring, Water Resour. Res., 45(4) (2009) 1-20.
27. A.K. Rai, A. Kumar, Continuous measurement of suspended sediment concentration: Technological advancement and future outlook, Measurement 76 (2015) 209-227.
28. C.P. Lin, C.C. Chung, I.L. Wu, P.L. Wu, C.H. Lin, C.H. Wu, Extensive monitoring system of sediment transport for reservoir sediment management, in: L.Wang, M.H. Wang, Y.T. Hung, N. Shammas (Eds.) Natural Resources and Control Processes. Handbook of Environmental Engineering 17. Springer, 2016, pp.449-492.
29. D.J. Law, A.J. Bale, S.E. Jones, Adaption of focused beam reflectance measurements to in situ particle sizing in estuaries and coastal waters, Marine Geology, 140 (1997), 47-59.
30. Y.C. Agrawal, H.C. Pottsmith, Laser diffraction particle sizing in STRESS, Cont. Shelf Res. 14 (10/11) (1994), 1101-1121.
31. V.K. Choubey, Monitoring water quality in reservoirs with IRS-1A-LISS-I, Water Resources Management 8 (1994), 121136
32. C.C. Chung, C.P. Lin, High concentration suspended sediment measurements using time domain reflectometry, Journal of hydrology 401(1) (2011) 134-144.
33. A. Scheuermann, Determination of Porosity Distributions of Water Saturated Granular Media Using Spatial Time Domain Reflectometry (Spatial TDR), Geotechnical Testing Journal 35 (3) (2012) 441-450.
34. D.R. Lucas, K. Fankhauser, S.M. Springman, Application of geotechnical and geophysical field measurements in an active alpine environment, *Eng. Geol.* 219 (2017) 32-51.
35. T. Bore, N. Wagner, C. Cai, A. Scheuermann, A. Broadband electromagnetic analysis of compacted kaolin, Measurement Science and Technology 28(1) (2016a) 014016.

36. C. Patriarca, F. Tosti, C. Velds, A. Benedetto, S. Lambot, E. Slob, Frequency dependent electric properties of homogeneous multi-phase lossy media in the ground-penetrating radar frequency range, Journal of Applied Geophysics 97 (2013) 81-88.

37. M.T. Hallikainen, F.T. Ulaby, M.C. Dobson, M.A. El-Rayes, L.K. Wu Microwave dielectric behavior of wet soil-part 1: Empirical models and experimental observations, IEEE Transactions on Geoscience and Remote Sensing 1 (1985) 25-34.
38. D.A. Robinson, S.B. Jones, J.M. Wraith, D. Or, S.P. Friedman, A review of advances in dielectric and electrical conductivity measurement in soils using time domain reflectometry, Vadose Zone Journal 2(4) (2003) 444-475.
39. A. Cataldo, L. Tarricone, F. Attivissimo, A. Trotta, Simultaneous measurement of dielectric properties and levels of liquids using a TDR method, Measurement 41 (2008) 307-319.
40. E. Piuzzi, E. Pittella, S. Pisa, A. Cataldo, E. De Benedetto, G. Cannazza, Microwave reflectometric methodologies for water content estimation in stone-made Cultural Heritage materials, Measurement (2017) https://doi.org/10.1016/j.measurement.2017.05.069
41. A. Sihvola, Mixing rules with complex dielectric coefficients. Subsurface sensing technologies and applications 1(4) (2000) 393-415.
42. A. Mortl, R. Muñoz Carpena, D. Kaplan, Y. Li, Calibration of a combined dielectric probe for soil moisture and porewater salinity measurement in organic and mineral coastal wetland soils, Geoderma 161 (2011) 50-62.
43. G. Kargas, P. Kerkides, Comparison of two models in predicting pore water electrical conductivity in different porous media, Geoderma 189-190 (2012) 563-573.
44. N.L.F. Ling, K.A. Kassim, A.T.A. Karim, Size Distribution Analysis of Kaolin using Laser Diffraction Technique, *Advanced Materials Research* 341-342 (2011) 108-112.
45. B.V.S. Viswanadham, Soil Mechanics Lectures by National Programme on Technology Enhanced Learning (NPTEL) http://nptel.ac.in/courses/105101084/7# (accessed on 26th Dec, 2016).
46. M. Schwing, Mechanical, hydraulic, and dielectric characterisation of fine-grained soils during densification, Ph.D. dissertation, School of Civil Engineering, The University of Queensland, Australia, 2015
47. P.N. Mishra, T. Bore, A. Scheuermann, L. Li, Measurement of dielectric properties

of Kaolin with saline pore fluid during dewatering, *in: 19th International Conference on Soil Mechanics and Geotechnical Engineering*, Seoul, South Korea, *2017b.*

48. H. Liu, H. Yang, F. Yi, Experimental study of the complex resistivity and dielectric constant of chrome-contaminated soil, Journal of Applied Geophysics 131 (2016) 109-116.
49. A.P. Gregory, R.N. Clarke, Dielectric metrology with coaxial sensors, Measurement Science and Technology 18(5) (2007) 1372–1386.
50. J.Z. Bao, C.C. Davis, M.L. Swicord, Microwave dielectric measurements of erythrocyte suspensions, Biophysical Journal 66(6) (1994) 2173–2180.
51. N. Wagner, M. Schwing, A. Scheuermann, Numerical 3d fem and experimental analysis of the open-ended coaxial line technique for microwave dielectric spectroscopy on soil, IEEE Transactions on Geoscience and Remote Sensing 52(2) (2014) 880–893.
52. F.M. Francisca, M.A. Montoro, Measuring the dielectric properties of soil–organic mixtures using coaxial impedance dielectric reflectometry, Journal of Applied Geophysics 80 (2012) 101-109.
53. W.J. Ellison, Permittivity of pure water, at standard atmospheric pressure, over the frequency range 0-25 THz and the temperature range 0-100 °C. *J. Phys. Chem. Ref. Data* 36(1) (2007) 1–18.
54. U. Kaatze, Reference liquids for the calibration of dielectric sensors and measurement instruments, Meas. Sci. Techno., 18 (18) (2007b) 967–976.
55. A.P. Gregory, R.N. Clarke, Tables of the complex permittivity of dielectric reference liquids at frequencies up to 5 GHz, NPL, New Delhi, India, Tech. Rep. MAT 23, 2009.
56. G.C. Topp, J.L. Davis, A.P. Annan, Electromagnetic determination of soil water content: Measurements in coaxial transmission lines, Water resources research 16(3) (1980) 574-582.
57. C.M. Regalado, R. Muñoz Carpena, A.R. Socorro, J.M. Herna´ndez Moreno,. Time domain reflectometry models as a tool to understand the dielectric response of volcanic soils, Geoderma 117 (2003) 313-330.
58. A.W. Western, M.S. Seyfried, A calibration and temperature correction procedure for the water-content reflectometer, Hydrological processes 19(18) (2005) 3785-3793.

59. T.J. Heimovaara, Frequency domain analysis of time domain reflectometry waveforms: 1. Measurement of the complex dielectric permittivity of soils, Water Resources Research 30(2) (1994) 189-199.

60. T. Bore, N. Wagner, S. Delepine Lesoille, F. Taillade, G. Six, F. Daout, D. Placko, Error analysis of clay-rock water content estimation with broadband high-frequency electromagnetic sensors - air gap effect, Sensors 16(4) (2016b) 554.

61. B. Bate, S.E. Burns, Complex dielectric permittivity of organically modified bentonite suspensions (0.2–1.3 GHz), Canadian Geotechnical Journal 51(7) (2014) 782-794.

62. M. Loewer, T. Günther, J. Igel, S. Kruschwitz, T. Martin, N. Wagner, Ultra-broadband electrical spectroscopy of soils and sediments–A combined permittivity and conductivity model, *Geophysical Journal International* 210 (3) (2017) 1360-1373

63. K. Lichtenecker, K. Rother, Die Herleitung des logarithmischenMis- chungsgesetzes aus allgemeinen Prinzipien der stationären Strömung, Physikalische Zeitschrift 32 (1931) 255–260.

64. P.N. Sen, C. Scala, M.H. Cohen, A self-similar model for sedimentary rocks with application to the dielectric constant of fused glass beads, Geophysics 46(5) (1981) 781–795.

65. Y. Chen, D. Or, Geometrical factors and interfacial processes affecting complex dielectric permittivity of partially saturated porous media,Water Resources Research, 42(6) (2006) 1-9.

66. U. Kaatze, Non-conducting and conducting reference liquids for the calibration of dielectric measurement systems, in: 7th International Conference on Electromagnetic Wave Interaction with Water and Moist Substances, ISEMA, Okamura, Japan, 2007a, pp.3-9.

67. M.C. Dobson, F.T. Ulaby, M.T. Hallikainen, M.A. El-Rayes, Microwave dielectric behavior of wet soil-part II: Dielectric mixing models, *IEEE Transactions on Geoscience and Remote Sensing* GE-23(1) (1985) 35–46.

68. J.A. Vrugt, Markov chain Monte Carlo Simulation Using the DREAM Software Package: Theory, Concepts, and MATLAB Implementation, Environ. Model. Softw. 75 (2016) 273-316.

69. W.K. Hastings, Monte Carlo sampling methods using Markov chains and their applications, Biometrika 57 (1970) 97–109.

70. P.N. Mishra, S. Suman, S.K. Das, Experimental investigation and prediction models for thermal conductivity of biomodified buffer materials for hazardous waste disposal.' J. Hazard. Toxic Radioact. Waste 21(2) (2017a) DOI: 10.1061/(ASCE)HZ.2153-5515.0000327
71. S.K. Das, N. Sivakugan, Discussion of: Intelligent computing for modeling axial capacity of pile foundations, *Can. Geotech. J.* 47 (2010) 928–930.
72. S.K. Das, S. Suman, Prediction of lateral load capacity of pile in clay using multivariate adaptive regression spline and functional network, *Arabian Journal for Science and Engineering* 40 (6) (2015) 1565–1578
73. R. Raythatha, P.N. Sen, Dielectric properties of clay suspensions in MHz to GHz range, J. Colloid Interface Sci. 109(2) (1986) 301–309.
74. T. Ishida, T. Makino, Microwave Dielectric Relaxation of Bound Water to Silica, Alumina, and Silica-Alumina Gel Suspensions. J. Colloid Interface Sci. 212(1) (1999) 144–151.
75. F.M. Francisca, V.I.C.A. Rinaldi, Complex dielectric permittivity of soil–organic mixtures (20 MHz–1.3 GHz).' *Journal of Environmental Engineering* 129(4) (2003) 347-357.

Figures

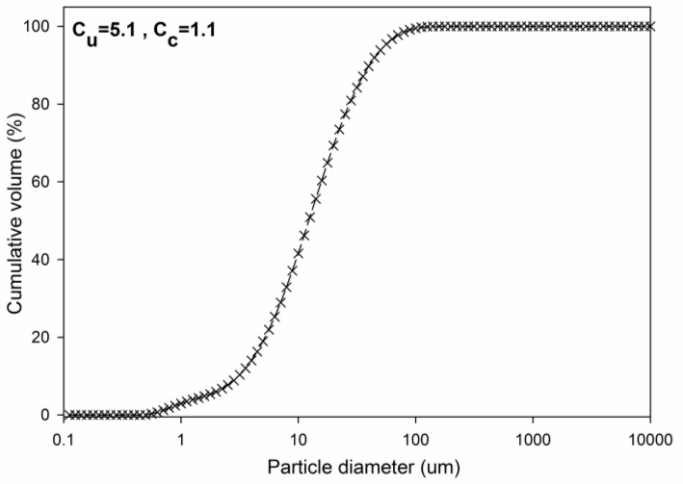

Fig. 1: Particle size distribution curve for kaolin (Eckalite-I)

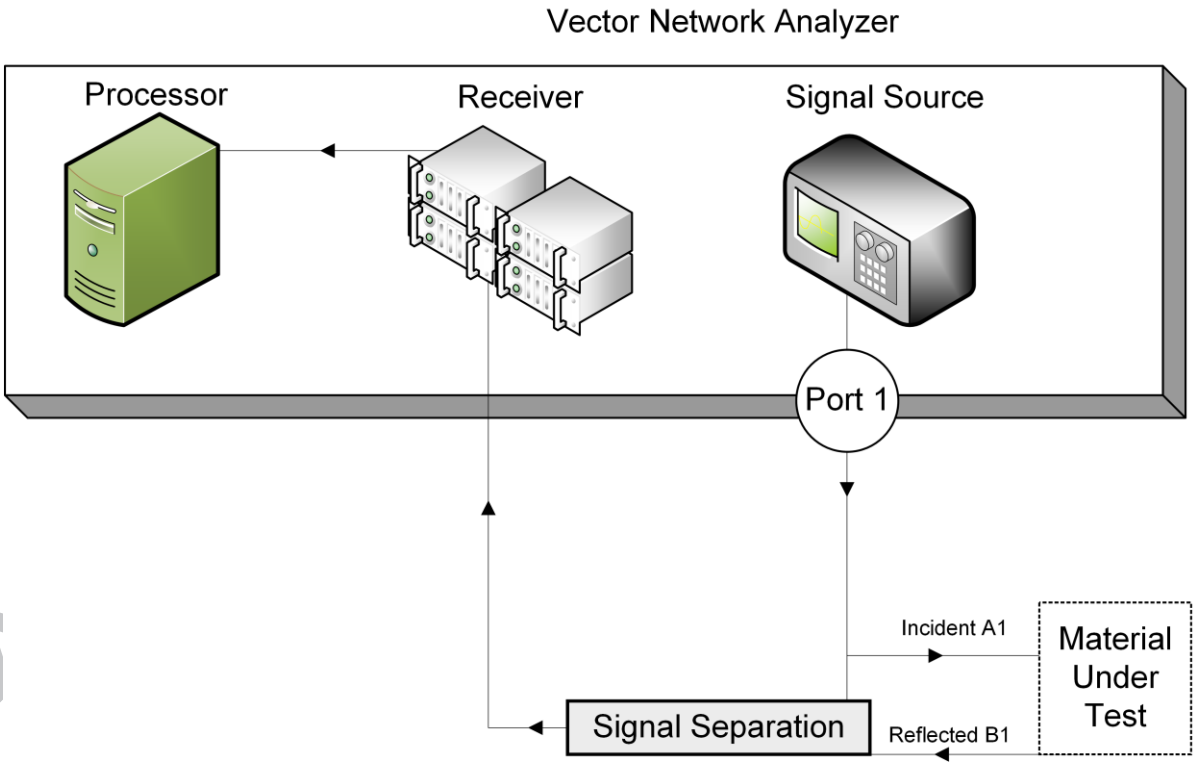

Fig. 2: Schematics of the VNA and one port measurement

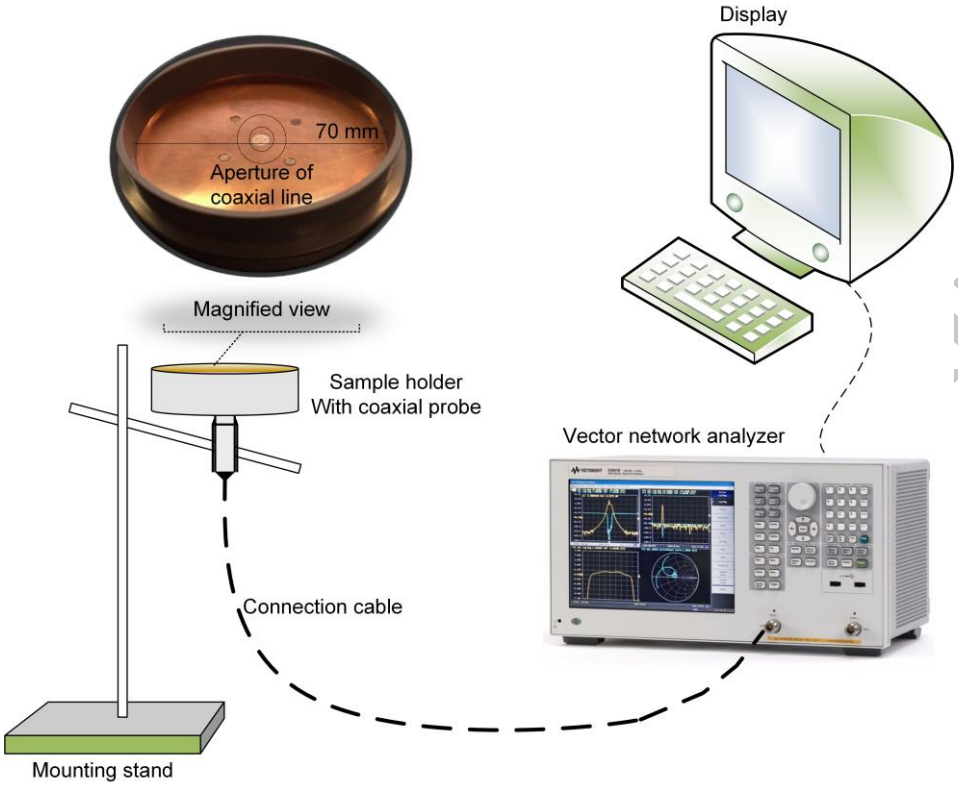

Fig. 3: In house experimental setup for frequncy dependent dielectric measurement

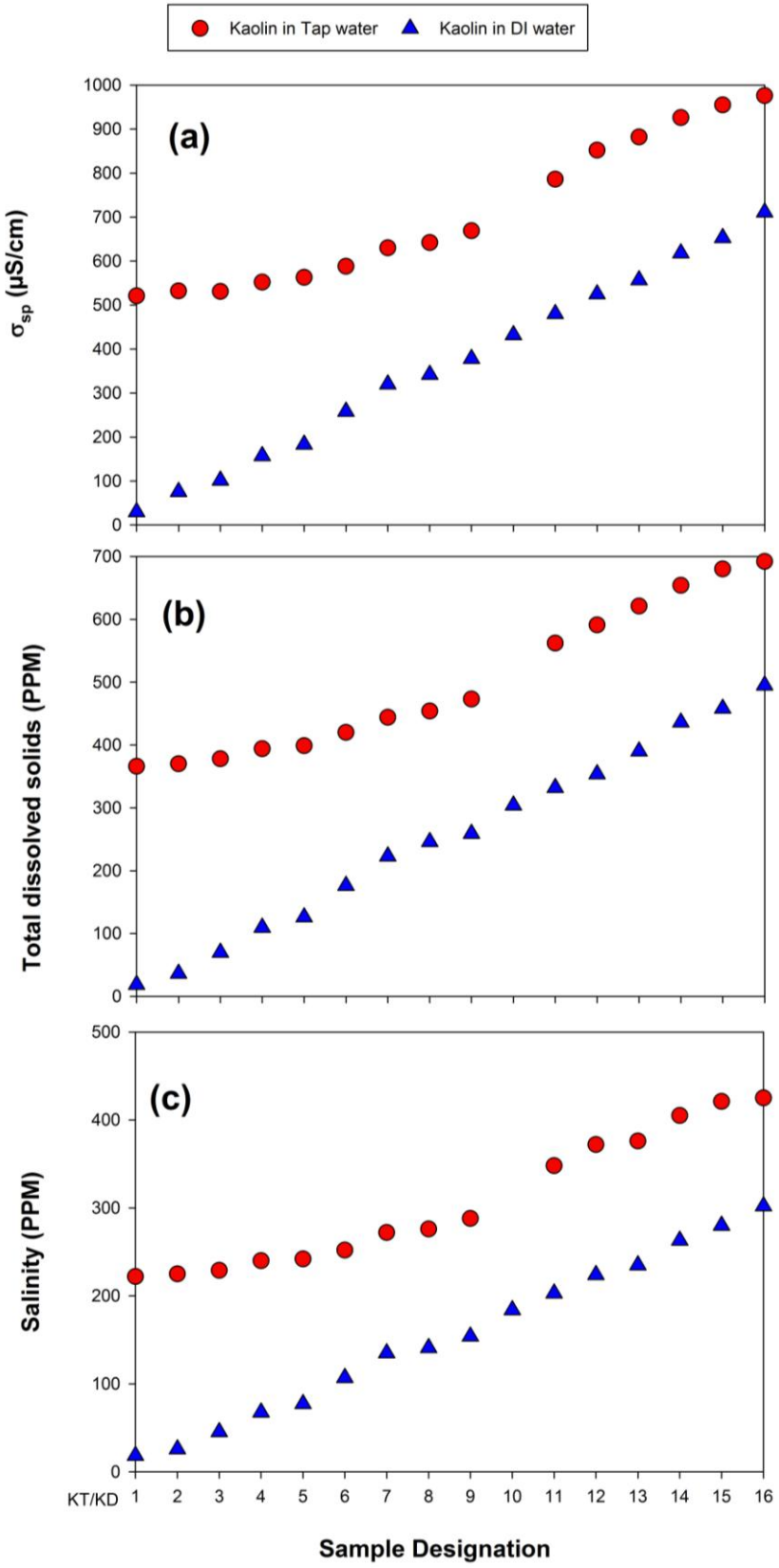

Fig 4: Measured parameters of the suspensions (a) σ_{sp} (b) TDS (c) salinity

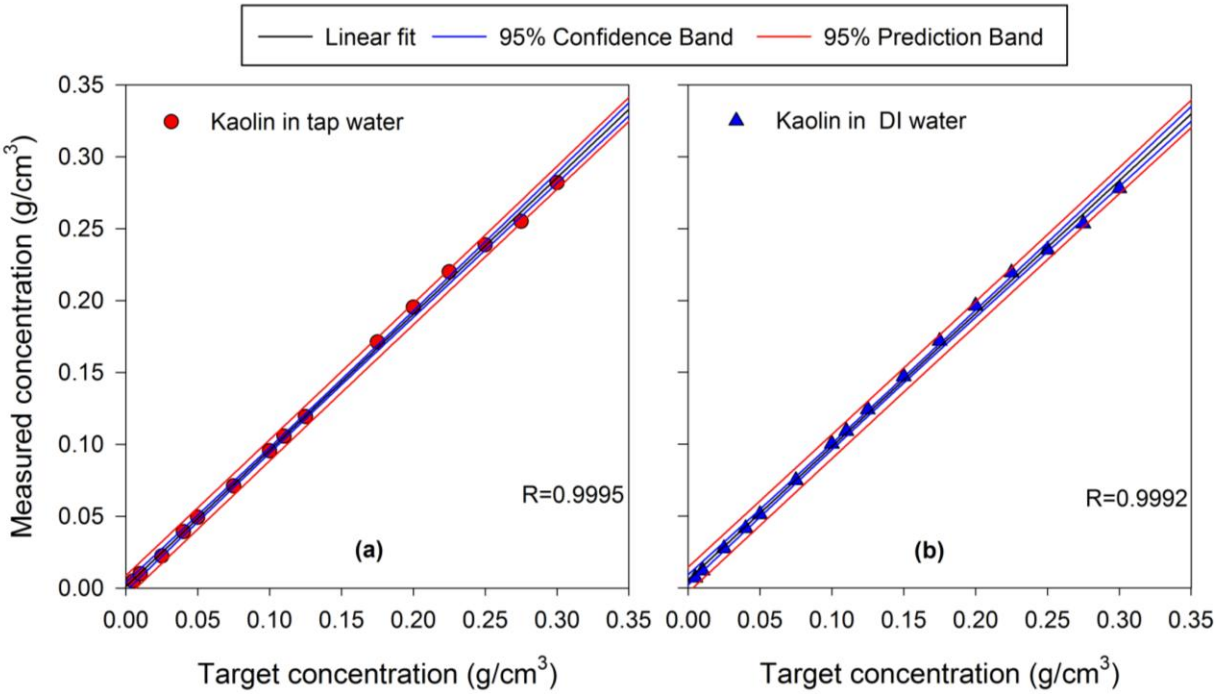

Fig 5: Target concentration vs. measured concentration for kaolin mixed with (a) tap water (b) DI water

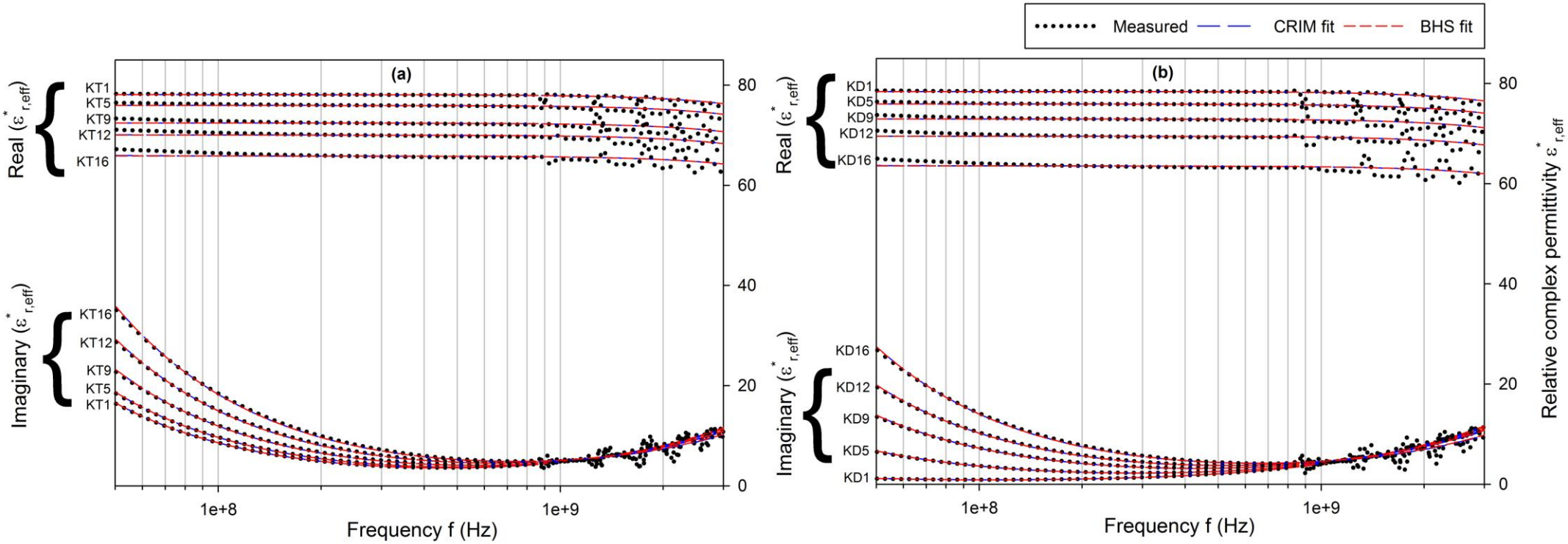

Fig 6: Evolution of relative complex permittivity over frequency for kaolin in (a) tap water (b) DI water

water

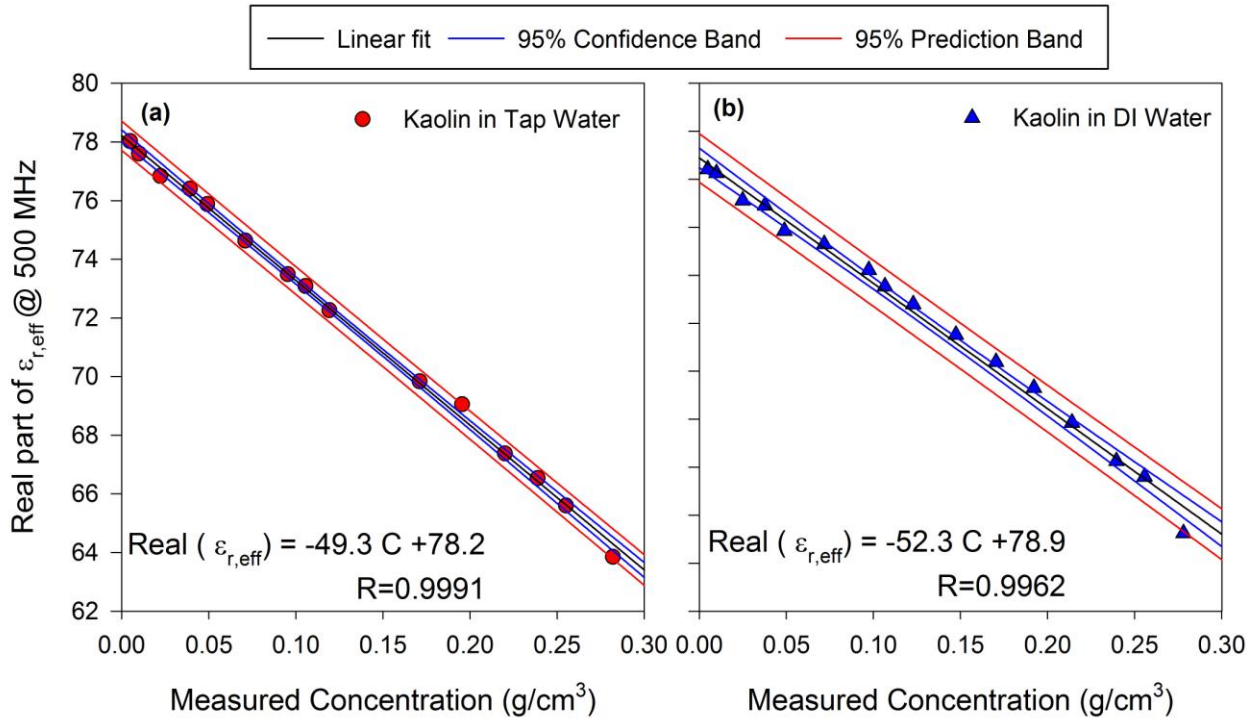

Fig 7: Correlating real part of $\varepsilon^*_{r,eff}$ at 500 MHz with measured concentration for kaolin in (a) tap water (b) DI water

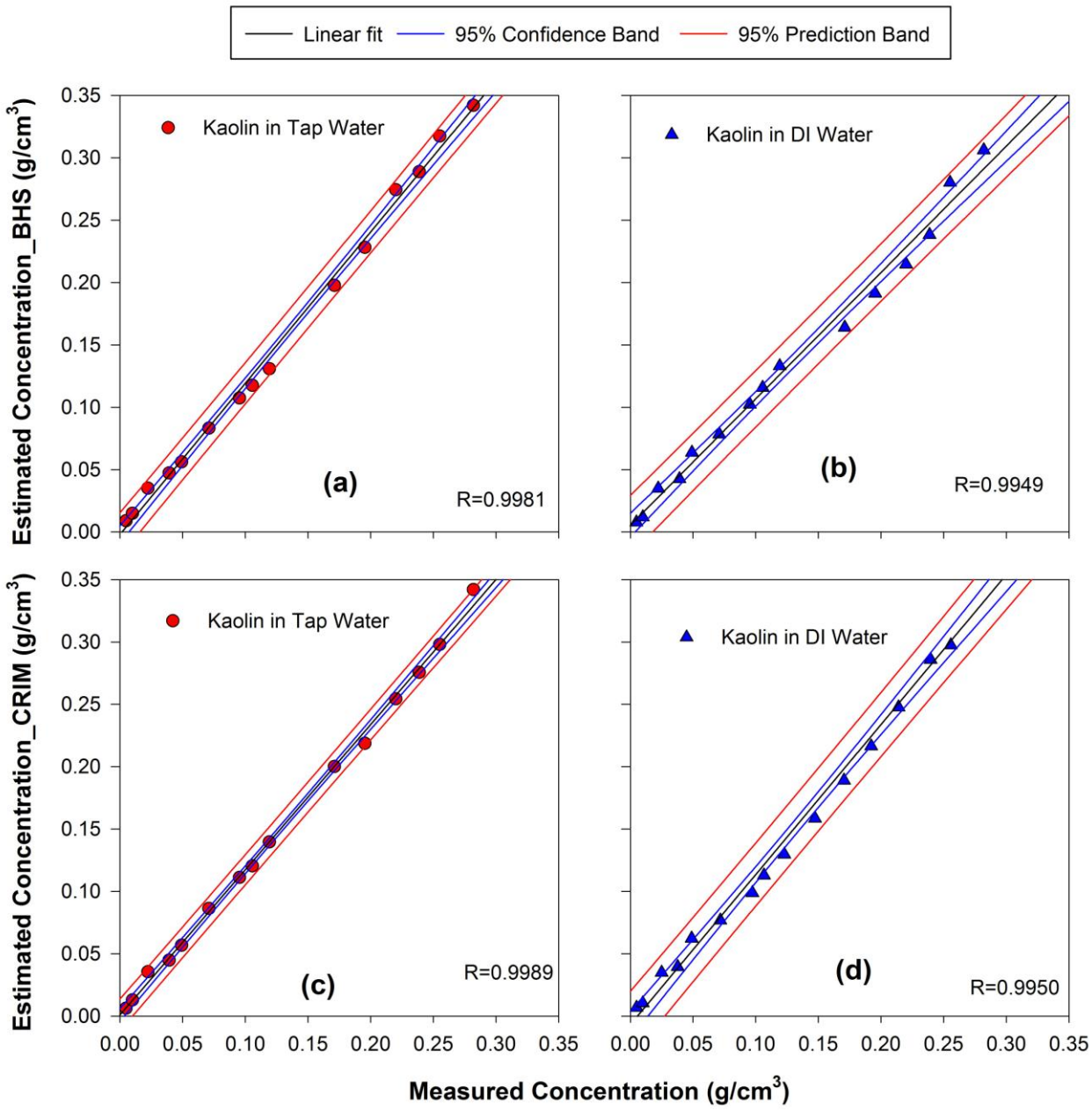

Fig 8: Estimated vs. measured concentration for kaolin in (a) tap water by BHS model (b) DI water by BHS model (c) tap water by CRIM (d) DI water by CRIM

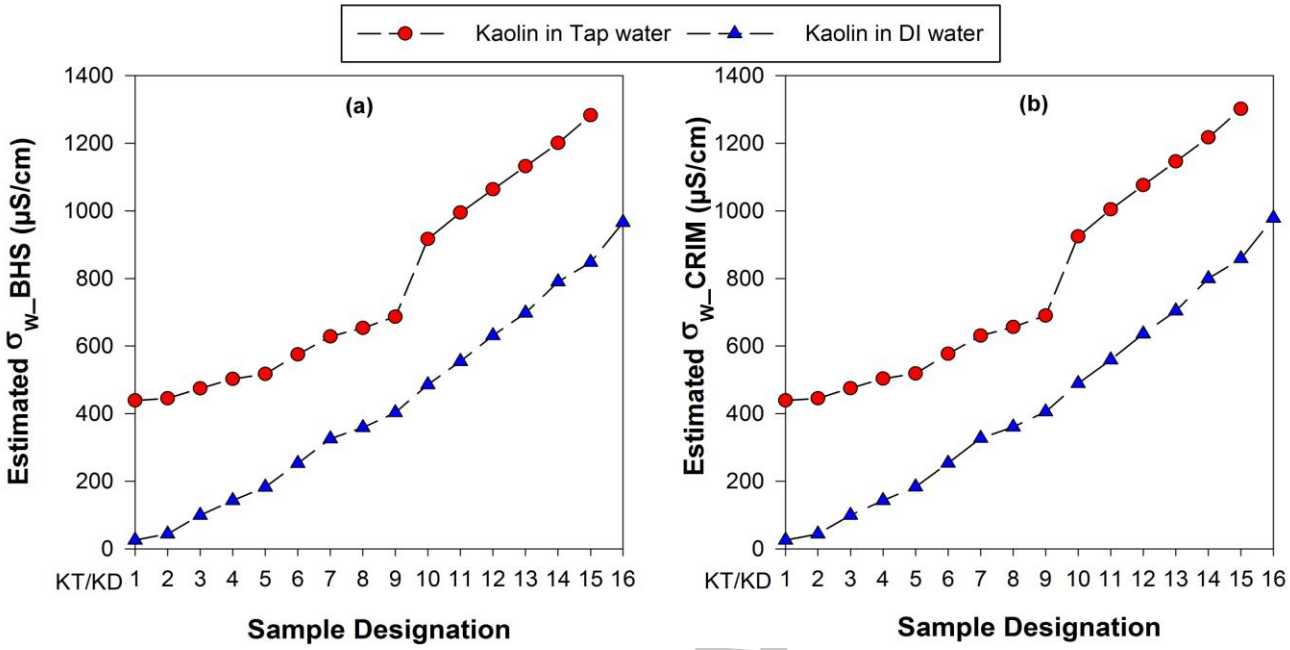

Fig 9: Estimated pore water conductivities by (a) BHS model (b) CRIM

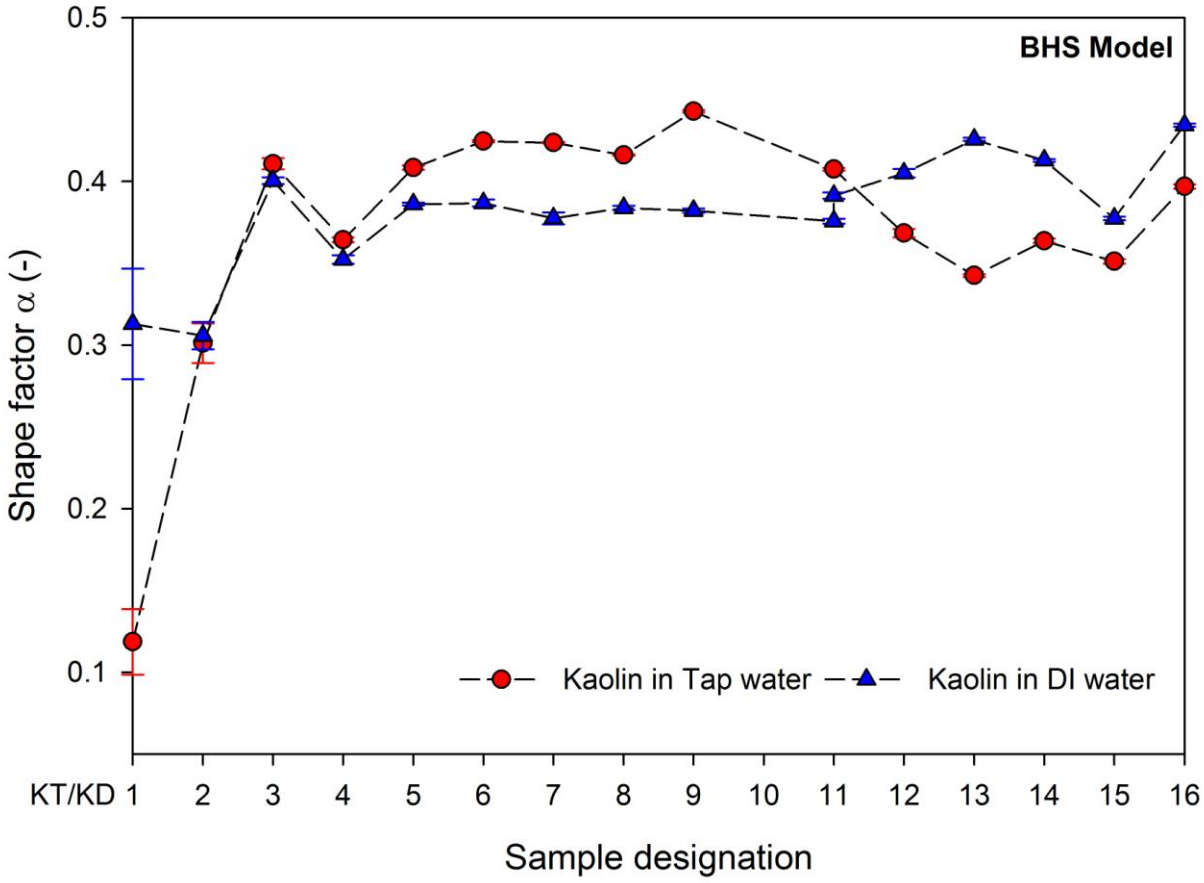

Fig 10: Estimated shape factors for the suspensions by BHS model

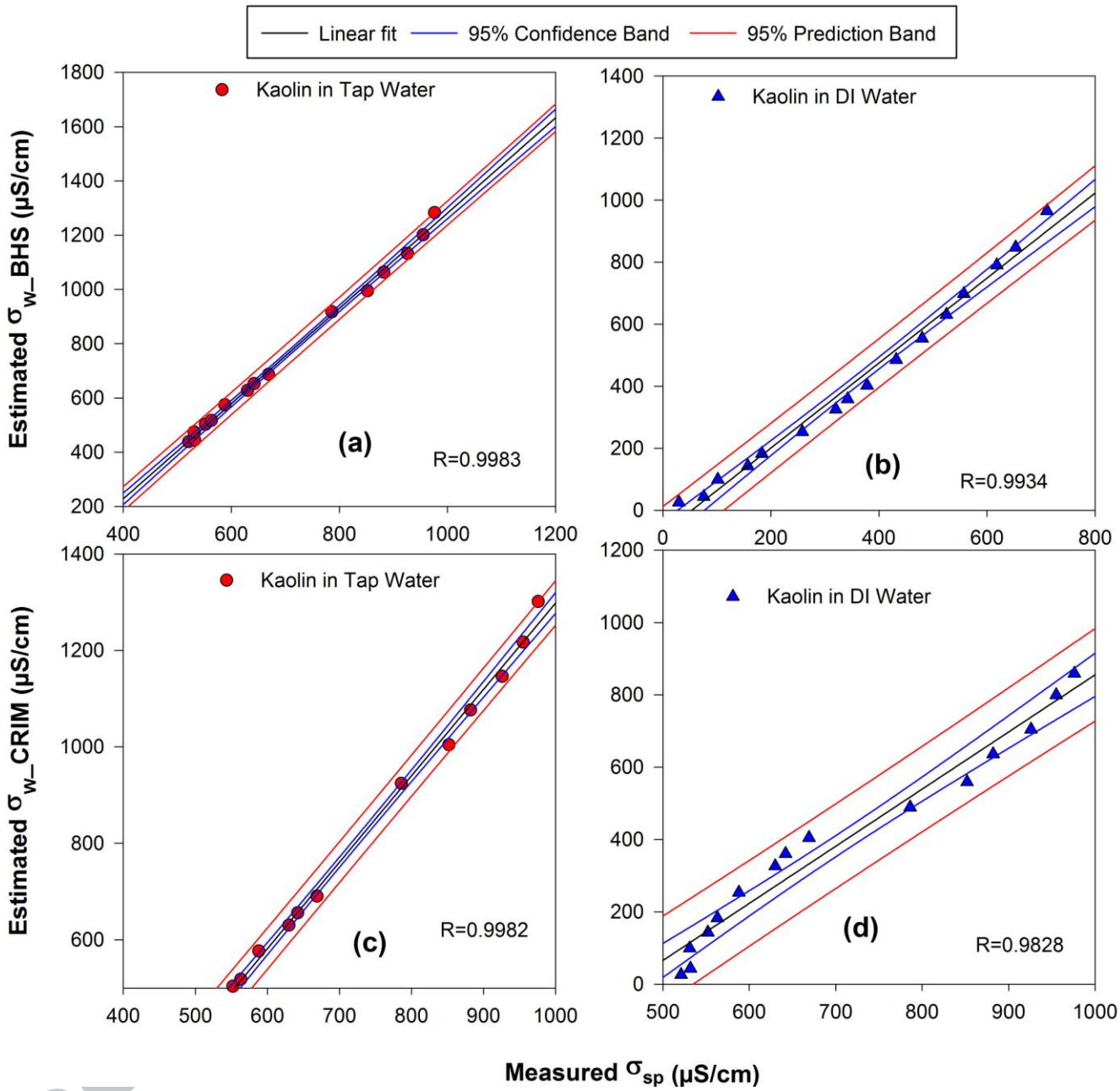

Fig 11: Estimated pore water conductivity vs. measured conductivity of suspension for kaolin in (a) tap water by BHS model (b) DI water by BHS model (c) tap water by CRIM (d) DI water by CRIM

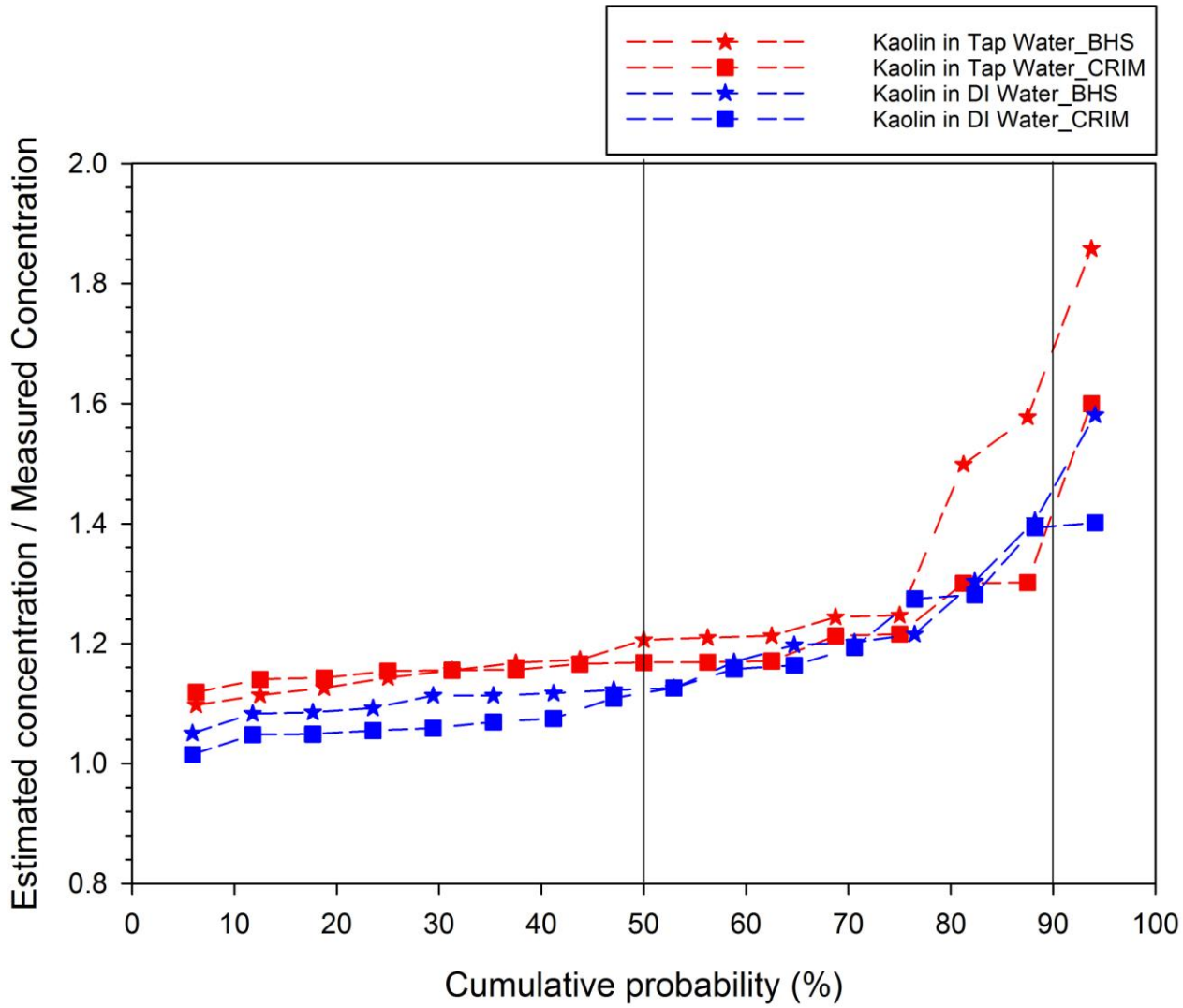

Fig 12: Plot of estimated/measured concentrations vs. cumulative probabilities

Tables

Table 1: Geotechnical parameters for kaolin (Schwing 2015)

Liquid limit (%)	Plastic limit (%)	Shrinkage limit (%)	Specific gravity	Plasticity index (%)
89.95	35.66	34.76	2.615	2.615

Table 2: Sample designations as per the target concentrations

Target concentration (g/cm^3)	Sample designation	
	Solvent phase	
	Tap water	Deionised water
0.005	KT1	KD1
0.010	KT2	KD2
0.025	KT3	KD3
0.040	KT4	KD4
0.050	KT5	KD5
0.075	KT6	KD6
0.100	KT7	KD7
0.110	KT8	KD8
0.125	KT9	KD9
0.150	_	KD10
0.175	KT11	KD11
0.200	KT12	KD12
0.225	KT13	KD13
0.250	KT14	KD14

0.275	KT15	KD15
0.300	KT16	KD16

Table 3: Ranking of Models

Solvent phase	**Model**	**Best fit calculation**			**Statistical calculations for the ratio of estimated to measured concentrations**			**Cumulative probability of the ratio of estimated to measured concentrations**			**Overall rank**	
		R	E	R1	μ	SD	R2	P_{50}	P_{90}	R3	RI	Final rank
Tap water	CRIM	0.9989	0.9193	1	1.211	0.120	1	1.17	1.42	1	3	1st
	BHS	0.9981	0.8849	2	1.269	0.212	2	1.21	1.64	2	6	2nd
DI water	CRIM	0.9950	0.9026	2	1.154	0.123	1	1.11	1.40	1	4	1st
	BHS	0.9949	0.9212	1	1.186	0.139	2	1.12	1.46	2	5	2nd

Dielectric Spectroscopy Measurements on Kaolin Suspensions for Sediment Concentration Monitoring

Highlights

- Dielectric spectroscopy aided suspended sediment concentration monitoring
- Correlations among frequency, permittivity and suspended sediment concentration
- Dielectric mixing equations for estimating suspended sediment concentration
- Statistical ranking model for judging relative efficiency of the mixing equations